High-Resistance Connection Detection in Induction Motor Drives Using Signal Injection

Pablo M. de la Barrera, *Member, IEEE*, Guillermo R. Bossio, *Member, IEEE*, and Jorge A. Solsona, *Senior Member, IEEE*

***Abstract*—Two new methods for high-resistance connection (HRC) diagnosis in induction motor (IM) drives are presented in this effort. These automatic offline methods are based on a signal injection strategy applied to the IM at standstill. By measuring the voltage in the machine neutral point and phase currents, it is possible to detect and isolate connection problems. Experimental results showing a good sensitivity to HRCs and immunity to symmetrical stator resistance variations were obtained in a laboratory setup.**

***Index Terms*—Fault diagnosis, high-resistance connection (HRC), induction motor (IM), signal injection.**

NOMENCLATURE

D	Duty cycle.
e	Percentage relative error.
I_0	Current offset.
i_a, i_b, i_c	Phase currents.
$\mathbf{i}_s$	Stator current vector.
$\bar{i}_y^{u_x}$	Mean value of i_y in the state u_x.
R_s	Symmetric stator resistance.
R_c	Connection resistance.
$\mathbf{r}_{\mathrm{HRC}}$	Resistance residual.
T_d	Dead time.
t_{off}	Period in which a zero state is applied.
t_{on}	Period in which an active state is applied.
T_s	Switching period.
V_0	Voltage offset.
v_a, v_b, v_c	Phase voltages.
$v_{b/c-a}$	Line-to-line voltage between phase b and phases c and a.
V_d	DC-link voltage.
$\mathbf{v}_{\mathrm{HRC}}$	Voltage residual.
v_m	Neutral point voltage.
$\mathbf{v}_s$	Stator voltage vector.
$\mathbf{v}_{\mathrm{se}}$	Exploratory signal voltage vector.
$\bar{v}_m^{u_x}$	Mean value of v_m in the state u_x.
Δ	Difference between ideal and actual signals.
ζ	Angle of the residual vector.
$\boldsymbol{\lambda}$	Limit value for the HRC alarm.
$^-$	Mean index.
$*$	Command index.

Manuscript received March 04, 2013; revised June 15, 2013; accepted July 28, 2013. Date of publication October 30, 2013; date of current version January 31, 2014. This work was supported in part by Universidad Nacional de Río Cuarto, by Universidad Nacional del Sur, by Fondo para la Investigación Científica y Tecnológica-Agencia Nacional de Promoción Científica y Tecnológica, and by Consejo Nacional de Investigaciones Científicas y Técnicas.

P. M. de la Barrera and G. R. Bossio are with the Grupo de Electrónica Aplicada, Facultad de Ingeniería, Universidad Nacional de Río Cuarto, X5804BYA Río Cuarto, Argentina, and also with Consejo Nacional de Investigaciones Científicas y Técnicas, Buenos Aires C1033AAJ, Argentina (e-mail: pbarrera@ieee.org; gbossio@ieee.org).

J. A. Solsona is with the Departamento de Ingeniería Eléctrica y de Computadoras, Instituto de Investigaciones en Ingeniería Eléctrica Alfredo Desages, Universidad Nacional del Sur, B8000CPB Bahía Blanca, Argentina, and also with Consejo Nacional de Investigaciones Científicas y Técnicas, Buenos Aires C1033AAJ, Argentina.

Color versions of one or more of the figures in this paper are available online at http://ieeexplore.ieee.org.

Digital Object Identifier 10.1109/TIE.2013.2278957

I. INTRODUCTION

RELIABILITY of induction motor (IM) is one of the most important topics in the industry due to its widespread use. In addition, they can cause unscheduled process downtimes, which produce important economical losses. Usually, these losses outweigh the cost of the motor maintenance [1]. For such reason, several fault detection and diagnosis methods based on currents, torque, power, vibration, or external magnetic flux, among other physical quantities, have been proposed [2]–[5].

The use of IM drives increases the stress on the machine and its power circuits. Electrical, mechanical, and thermal stresses appear on the windings, bearings, and stator core of the IM, increasing the possibilities of failures [6], [7].

Power circuits include all conductors and connections between the power source and the IM. As it was expressed in [8], 46% of the faults that reduce the motor efficiency are produced in power circuits, where connection problems are the most important (approximately 80% of the power circuit problems).

High-resistance connection (HRC) is a typical progressive fault whose mechanism can be schematized by the diagram in Fig. 1 [9]. It represents the way in which some factors (e.g., high current or voltage, vibration, chemicals or dirt in the atmosphere, metal fatigue, aging, or extreme ambient temperature) can initiate the degradation mechanism. It is characterized by two main positive feedback loops where the contact resistance increment produces contact temperature rise. This temperature increment produces thermal expansion (and the subsequent stress relaxation and creep) and the acceleration of oxidation and/or corrosion. The aforementioned effects cause an increase in contact resistance; thereby, the positive feedback loops for the degradation of a power connection are closed.

If these loops are not broken, it can result in uncontrollable overheating. It would be the precursor of arc flash, connection and cable melting, and even an electrical fire, causing equipment and building losses as well as personal injuries [10].

The increment in the contact resistance also produces an unbalanced supply voltage of the IM, in which, if the IM is

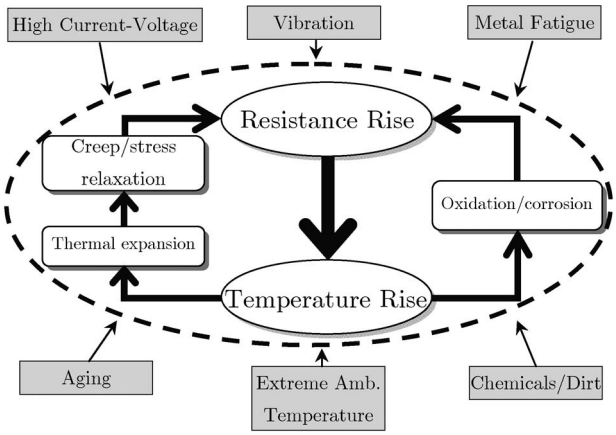

Fig. 1. Simplified scheme of degradation mechanism for power connections.

fed by an inverter, two possible scenarios would be present [11]–[14].

1) Open-loop drives are usually based on a scalar v/f control method, which imposes a balanced voltage to the IM through the inverter. In this case, an asymmetry in the IM phases (stator turn fault or increase in contact resistance) produces similar effects as those in an IM fed by the grid. That is, negative sequence currents flow in the IM, which, in addition, produce an oscillating torque at twice the grid frequency while reducing the IM efficiency. These additional mechanical and thermal stresses accelerate the deterioration of the IM winding isolation leading to a failure.
2) In case of closed-loop drives, the effects produced by a stator asymmetry over the IM are very different compared with the open-loop drives. Closed-loop drives cover some typical characteristics produced by a stator asymmetry (negative sequence current and oscillating torque) due to its current and speed regulators, thereby increasing the complexity of the analysis and interpretations of the results [12], [13].

Fault diagnosis methods for open-loop IM drives have been developed based on methods proposed for IM supplied from the grid. Nevertheless, these methods are not convenient in practice due to the variable operation condition (speed or torque) of IM drives [13]. In addition, these proposed methods also fail when closed-loop drives are used due to the different effects produced by them when a fault appears. Therefore, new diagnosis methods devoted to IM drives have been developed [15], [16].

Moreover, in order to overcome these problems, diagnosis methods based on high-frequency signal injection (HFSI) have been deeply studied and proposed throughout the last decade. HFSI has been used for position estimation in electric motor drives at low speed, e.g., [17]–[20]. These methods are based on tracking the position of some constructive rotor asymmetries or saturation [21], [22].

HFSI has been used for the diagnosis of many different IM faults, namely, air-gap eccentricity [23], broken rotor bars [24], winding turn faults [12], [25], [26], and stator core faults [6], [27]. Although these methods are widely used in the diagnosis area, to the best of the authors' knowledge, only one method for HRC diagnosis based on HFSI suitable for IM drives has been reported in literature [15].

The most widespread methods for HRC are the voltage drop survey and the infrared thermography [9], [28]. The first one is a simple, quick, and cheap method based on comparing the magnitude of the voltage drop in each phases in the loaded IM in order to detect HRC. An important disadvantage is the personal risk associated to measurement processes since an operator must perform it with the fed IM.

Infrared thermography is a quick and reliable method for detecting hot spots in different IM drive components. A disadvantage of this method is the cost of the infrared camera as well as those associated to the plant inspection and the postprocessing of the images. All these tasks must be performed by a specialist, with the automation of the detection and diagnosis process being difficult. Other methods based on artificial intelligence [29], upstream impedance measurement [30], and sequence components [8], [31] have been presented but only for IM fed by the grid.

Recently, two new strategies for the detection of stator dissymmetry in drives with multiphase IMs [32] and wound rotor induction machines [33] have been proposed. These strategies can detect HRCs. However, the isolation of other stator faults in the IM presents unresolved issues.

Therefore, two new offline HRC diagnosis methods using HFSI are presented in this paper. A unipolar predefined signal is injected to the power circuits of the IM at standstill condition. The effect of this signal is analyzed using a new fault indicator, which is calculated by using a single voltage sensor, measuring the dc-link negative voltage with respect to the IM neutral point. A second fault indicator is proposed in case IM phase current information is available. Both options were experimentally validated in a laboratory, demonstrating good performance and sensitivity to the HRC while showing immunity to symmetric variations of IM stator resistance as well as stator winding turn fault (which produces inductance variations). In addition, based on these new fault indicators, a fault detection and isolation (FDI) algorithm is proposed, and the methodology to determine limits for the HRC alarms is presented.

The approach presented in this paper can be combined with previous proposals based on HFSI, which use the information of neutral point voltage [23], [24], [26]. It allows detecting and isolating broken rotor bars, eccentricity, shorted turns, and HRC in the IM.

This paper is organized as follows. Section II presents the two methods for HRC diagnosis using HFSI. The experimental setup and the obtained results are presented in Section III. Section IV presents the FDI algorithm proposed for diagnosing HRC problems. Finally, some conclusions and final remarks are drawn in Section V.

II. HRC Diagnosis Methods

Two methods to diagnose HRC are presented here. The first one used the information of a single voltage sensor. The second one, in addition to the single voltage, used the phase current information. A detailed description of each method is presented in the following subsections.

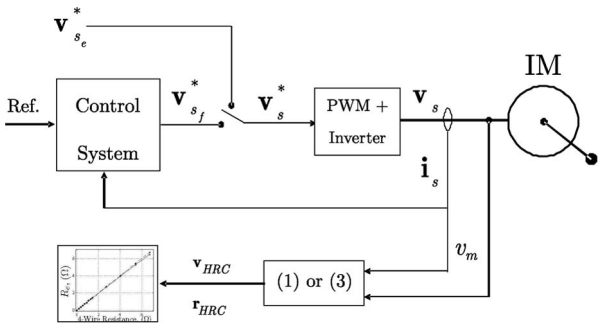

Fig. 2. Block diagram of the HRC diagnosis method.

A. Using a Single Voltage Sensor

The proposed method is based on the effects caused by HRC over a determined voltage signal, when the IM is excited by a predefined unipolar pulse sequence (exploratory signal) imposed by a three-phase inverter. This one is an offline method since the exploratory signal is injected when the IM is at standstill, applying this method in each process scheduled downtime.

A block diagram of the proposed method is presented in Fig. 2. It is observed that the exploratory signal, i.e., $\mathbf{v}^*_{\mathrm{se}}$, is injected when the control loop is opened.

Fig. 3(a) shows the scheme of the inverter (connected with the IM) where the only voltage sensor, used by this approach, measures the dc-link negative voltage with respect to the IM neutral point, i.e., v_m. This sensor arrangement is the same as the one proposed in [26] and [27] for the diagnosis of stator core and winding turn faults, respectively.

The exploratory signal is composed of three of the six active states of the three-phase inverter, namely, $u_4(-++)$, $u_6(+-+)$, and $u_2(++-)$ [see Fig. 3(b)], and a zero state $u_0(---)$. A representation of the IM windings connection for each of the active states is presented in Fig. 3(c)–(e). In addition, the measured voltage is indicated in these figures. From these figures, it is possible to observe that, when u_4 is injected, v_m measures the voltage in phase a, whereas when u_6 and u_2 are injected, voltages in phases b and c, respectively, are measured. Fig. 4 shows the pulse sequence for the upper switches of the inverter (S_1, S_2, and S_3). The figure is divided into three parts, one for each phase, in which the sequences of the active and zero states are shown (SS in the figure). Therefore, it is possible to measure the voltage in each phase using only a single voltage sensor when the signal $\mathbf{v}^*_{\mathrm{se}}$ is injected.

Based on this fact, the following signal is proposed as a residual:

$$\mathbf{v}_{\mathrm{HRC}} = \bar{v}_m^{u_4}\,\hat{\mathbf{i}} + \bar{v}_m^{u_6}\,\hat{\mathbf{j}} + \bar{v}_m^{u_2}\,\hat{\mathbf{k}} \tag{1}$$

where $\bar{v}_m^{u_x}$ represents the mean value of v_m in the state u_x; $\hat{\mathbf{i}}$, $\hat{\mathbf{j}}$, and $\hat{\mathbf{k}}$ are the versors in the following directions:

$$\hat{\mathbf{i}} = \begin{bmatrix} 1 \\ 0 \end{bmatrix};\ \hat{\mathbf{j}} = \begin{bmatrix} \cos\left(\frac{2}{3}\pi\right) \\ \sin\left(\frac{2}{3}\pi\right) \end{bmatrix};\ \hat{\mathbf{k}} = \begin{bmatrix} \cos\left(-\frac{2}{3}\pi\right) \\ \sin\left(-\frac{2}{3}\pi\right) \end{bmatrix}. \tag{2}$$

This way, if the IM is symmetrical, $\mathbf{v}_{\mathrm{HRC}}$ is equal to the null vector since the values of $\bar{v}_m^{u_4}$, $\bar{v}_m^{u_6}$, and $\bar{v}_m^{u_2}$ are equal. Given that the IM has inherent asymmetries, there is a limit for $\mathbf{v}_{\mathrm{HRC}}$, which is represented by a circumference in Fig. 5. If the Euclidean norm of $\mathbf{v}_{\mathrm{HRC}}$ is smaller than that limit, IM inherent asymmetries could be present. In addition, (1) gives information about the direction of the HRC, allowing its physical location.

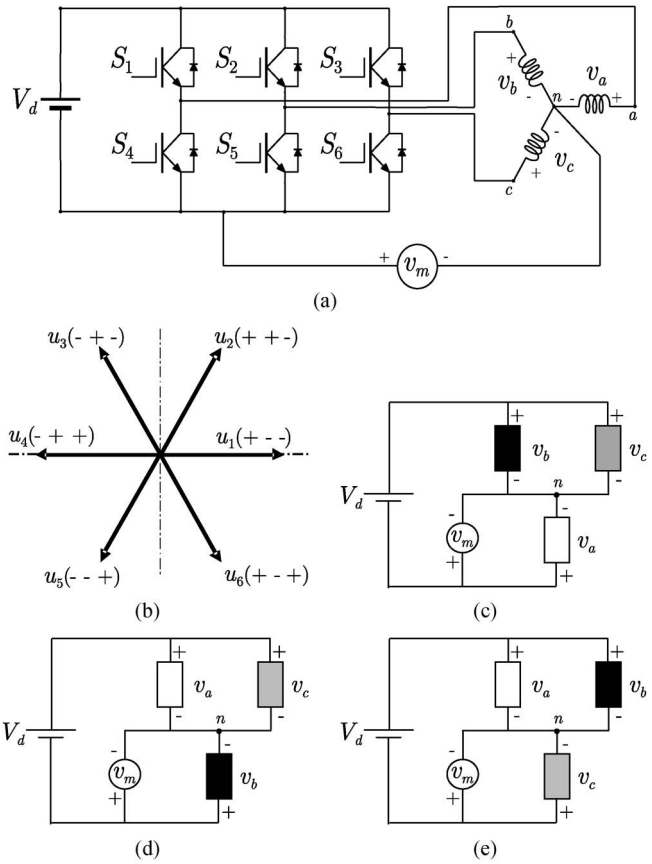

Fig. 3. (a) Three-phase inverter and IM connection. (b) Active state vectors. (c) u_4 state. (d) u_6 state, and (e) u_2 state.

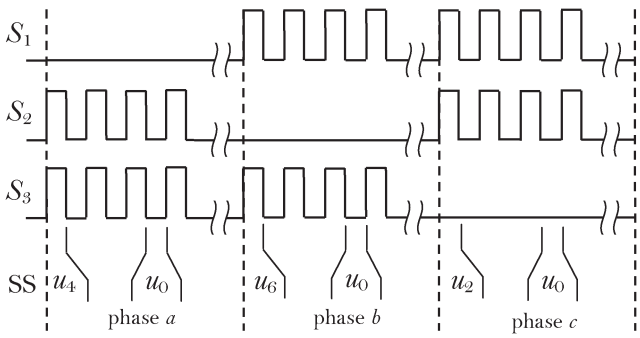

Fig. 4. Sequence signals for upper switches.

An important advantage of this residual is its low sensitivity to inductance variations produced by other IM asymmetries (e.g., stator winding turn faults or air-gap eccentricities) due to the fact that it is calculated from the mean values of the measured voltage. In addition, previous papers [23], [26] present HFSI diagnosis methods for stator winding turn faults and air-gap eccentricities whose proposed fault indicators have a very low sensitivity to resistance variations [26]. Therefore, the combined use of previous works and the one proposed in this paper for HRC detection would separate these types of faults for a correct diagnosis.

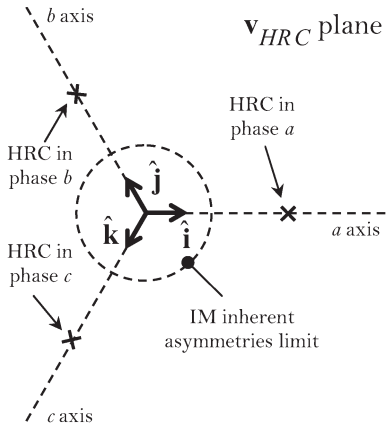

Fig. 5. Plane of the possible values of $\mathbf{v}_{\mathrm{HRC}}$.

B. Using a Single Voltage Sensor and the Phase Current Information

Current sensors are usually incorporated in IM drives. Generally, open-loop drives do not need phase current information, whereas closed-loop drives use current signals for the control. Therefore, if the information of those sensors is available, it is possible to modify the previous method to obtain the following new fault indicator:

$$\mathbf{r}_{\mathrm{HRC}} = \begin{pmatrix} \bar{v}_m^{u_4} \\ \bar{i}_a^{u_4} \end{pmatrix} \hat{\mathbf{i}} + \begin{pmatrix} \bar{v}_m^{u_6} \\ \bar{i}_b^{u_6} \end{pmatrix} \hat{\mathbf{j}} + \begin{pmatrix} \bar{v}_m^{u_2} \\ \bar{i}_c^{u_2} \end{pmatrix} \hat{\mathbf{k}} \tag{3}$$

where $\bar{i}_y^{u_x}$ represents the mean value of i_y in the state u_x.

As an example, if a symmetrical IM, whose stator resistance values are R_s, and an HRC in the phase a of the motor incoming circuits (R_c) are considered, the following expressions are obtained:

$$\begin{pmatrix} \bar{v}_m^{u_4} \\ \bar{i}_a^{u_4} \end{pmatrix} = R_s + R_c;\ \begin{pmatrix} \bar{v}_m^{u_6} \\ \bar{i}_b^{u_6} \end{pmatrix} = R_s;\ \begin{pmatrix} \bar{v}_m^{u_2} \\ \bar{i}_c^{u_2} \end{pmatrix} = R_s \tag{4}$$

yielding the following fault indicator:

$$\mathbf{r}_{\mathrm{HRC}}|_{ex} = \begin{bmatrix} R_c \\ 0 \end{bmatrix}. \tag{5}$$

This example shows that if a symmetric change in the stator resistance occurs, (e.g., produced by temperature increment) the fault indicator is not affected by this change. The same analysis can be performed if the conduction equivalent resistances of the inverter switches (r_{CEon} for IGBTs and R_{DSon} for MOSFETs) are considered, yielding similar results. Therefore, it is possible to assert that the proposed fault indicator has a low sensitivity to symmetrical variations of stator resistance or equivalent resistance of switching elements.

C. Effect of Dead Time

Here, a brief analysis of the dead time effects over the proposed method is presented.

These effects are analyzed by comparing the ideal and actual line voltages of the IM when phase a is excited, i.e., u_4 is injected. Due to dead time T_d, the ideal line voltage $v_{b/c-a}^{\mathrm{ideal}}$ becomes $v_{b/c-a}^{\mathrm{actual}}$, as shown in Fig. 6. In this case, dead time is presented during the transition from t_{off} to t_{on}; this fact can be seen by analyzing the channel flow of the current in phase a, as it was shown in [34] and [35]. As a result, the difference between the ideal and actual line voltages is represented by $\Delta v_{b/c-a}\ (= v_{b/c-a}^{\mathrm{ideal}} - v_{b/c-a}^{\mathrm{actual}})$.

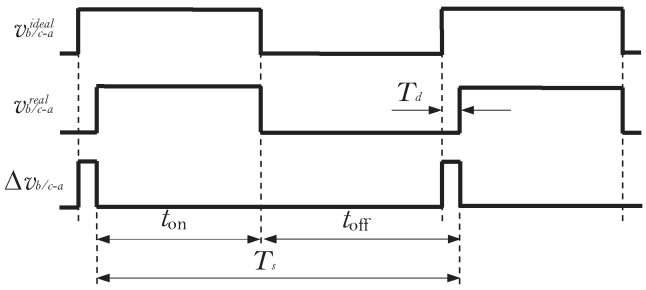

Fig. 6. Relationship between ideal and actual IM line voltages.

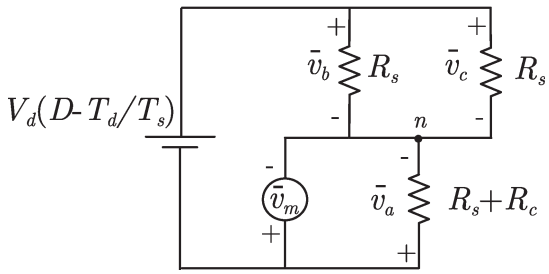

Fig. 7. Simplified equivalent circuit during u_4 injection.

By analyzing Fig. 6, it is possible to infer that dead time affects the mean value of the line voltage $\bar{v}_{b/c-a}$ of the IM. $\bar{v}_{b/c-a}$ can be calculated as follows:

$$\bar{v}_{b/c-a} = \frac{V_d\, t_{\mathrm{on}} - V_d\, T_d}{T_s} = \left(D - \frac{T_d}{T_s}\right) V_d \tag{6}$$

where V_d is the dc-link voltage, and D represents the duty cycle.

Fig. 7 shows a simplification of the circuit shown in Fig. 3(a). This simplification considers the mean values of the voltages and currents during u_4 injection. In addition, an HRC is considered in phase a (R_c).

The expression of $\bar{v}_m^{u_4}$ can be derived by inspection from Fig. 7 as

$$\begin{aligned} \bar{v}_m^{u_4} &= \left[\frac{\left(D - \frac{T_d}{T_s}\right) V_d}{\frac{R_s}{2} + R_s + R_c}\right] (R_s + R_c) \\ &= V_d \left(D - \frac{T_d}{T_s}\right) \left(\frac{2R_s + 2R_c}{3R_s + 2R_c}\right). \end{aligned} \tag{7}$$

In the same way, it is possible to analyze the equivalent circuits during u_6 and u_2 injection, obtaining the following expressions:

$$\bar{v}_m^{u_6} = V_d \left(D - \frac{T_d}{T_s}\right) \left(\frac{2R_s + R_c}{3R_s + 2R_c}\right) \tag{8}$$

$$\bar{v}_m^{u_2} = \bar{v}_m^{u_6}. \tag{9}$$

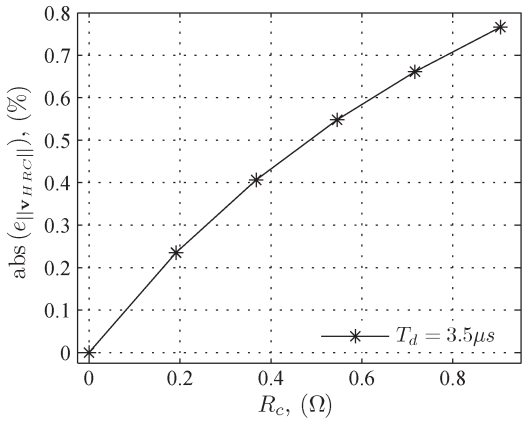

Fig. 8. $e_{\|\mathbf{v}_{\mathrm{HRC}}\|}$ as a function of contact resistances considering the dead time effect.

TABLE I
INVERTER AND IM RATED VARIABLES AND PARAMETERS

Inverter		
Semikron SKiip 232GDL 120-410CTV		
Variable/Parameter	Value	Unit
V_d	100	(V)
T_d	3.5	(μs)
T_s	750	(μs)
D	0.1	-
IM		
Power (P_n)	5.5	(kW)
Line Voltage (V_n)	380	(V)
Current (I_n)	11	(A)
Frequency (f_n)	50	(Hz)
Torque (T_e)	35	(Nm)
Poles (P)	4	-
R_{sa}	0.951	
R_{sb}	0.932	(Ω)
R_{sc}	0.911	
R_s =mean($[R_{sa}, R_{sb}, R_{sc}]$)	0.9313	(Ω)

If (7)–(9) are substituted in (1), the residual use to diagnose the HRC, which considers the effect of T_d, is obtained. In order to quantify this effect, the percentage relative error between $\|\mathbf{v}_{\mathrm{HRC}}\|$ with and without T_d can be calculated as

$$e_{\|\mathbf{v}_{\mathrm{HRC}}\|} = \frac{\|\mathbf{v}_{\mathrm{HRC}}\|_{(T_d=0)} - \|\mathbf{v}_{\mathrm{HRC}}\|_{(T_d)}}{V_d D} \times 100\%. \quad (10)$$

Fig. 8 shows the absolute value of the error as a function of R_c. These theoretical results were obtained under the following considerations.

1) T_d was set in the value given by the used inverter in the experimental setup. In the same way, T_s, V_d, and D were set based on the values of the experimental setup.
2) For simplicity, the same value of winding resistance R_s was assumed in the three phases, and it was set equal to the mean value between the three phases.

Table I shows the values of mentioned parameters and some information about the used inverter and IM.

From Fig. 8, it is observed that T_d produces a small variation of the residual (less than 1% for the worst case of R_c), at least for the selected inverter and IM parameters presented in this paper. Therefore, henceforth dead time will not be taken into account for the next theoretical analysis.

D. Effect of Sensor's Offset

The effect of offset in the voltage and current sensors over the proposed methods is analyzed here.

First, it is considered an offset in the voltage sensor, indicated as V_0. In this condition, the measured voltages in each state are given by

$$\begin{aligned}\bar{v}_m^{u_4}|_0 &= \bar{v}_m^{u_4} + V_0\\ \bar{v}_m^{u_6}|_0 &= \bar{v}_m^{u_6} + V_0\\ \bar{v}_m^{u_2}|_0 &= \bar{v}_m^{u_2} + V_0.\end{aligned}$$

Replacing previous equations in (1), the following expression is obtained:

$$\mathbf{v}_{\mathrm{HRC}}|_0 = \bar{v}_m^{u_4}\,\hat{\mathbf{i}} + \bar{v}_m^{u_6}\,\hat{\mathbf{j}} + \bar{v}_m^{u_2}\,\hat{\mathbf{k}} + V_0\left(\hat{\mathbf{i}} + \hat{\mathbf{j}} + \hat{\mathbf{k}}\right) \quad (11)$$

where the last term of (11) is identically zero. Therefore, it can be asserted that the residual $\mathbf{v}_{\mathrm{HRC}}$ is not affected by the offset in the voltage sensor.

For the second method, the same analysis can be performed when an offset in one of the current sensors is considered. The measured currents are given by

$$\begin{aligned}\bar{i}_a^{u_4}|_0 &= \bar{i}_a^{u_4}\\ \bar{i}_b^{u_6}|_0 &= \bar{i}_b^{u_6} + I_0\\ \bar{i}_c^{u_2}|_0 &= -\left(\bar{i}_a^{u_2} + \bar{i}_b^{u_2} + I_0\right)\end{aligned}$$

where I_0 represents the offset in the current sensor of phase b. Replacing previous equation in (3), the following expression is obtained:

$$\mathbf{r}_{\mathrm{HRC}}|_0 = \left(\frac{\bar{v}_m^{u_4}}{\bar{i}_a^{u_4}}\right)\hat{\mathbf{i}} + \left(\frac{\bar{v}_m^{u_6}}{\bar{i}_b^{u_6} + I_0}\right)\hat{\mathbf{j}} - \left(\frac{\bar{v}_m^{u_2}}{\bar{i}_a^{u_2} + \bar{i}_b^{u_2} + I_0}\right)\hat{\mathbf{k}}. \quad (12)$$

By analyzing (12), it can be observed that the offset in one of the two current sensors affects the residual $\mathbf{r}_{\mathrm{HRC}}$, and it must be taken into account when the proposed method is applied. Two strategies can be adopted in order to avoid current offset. The first one is by compensating this offset, which can be measured in a previous step to the application of the proposed method. The second one is based on the use of a dc-link current sensor. If this sensor is available, it allows measuring the current in the phase, which is excited by the active vector of the inverter. Hence, if the dc-link current sensor has an offset, it is canceled in the same way shown for an offset in the voltage sensor.

Based on comments from previous discussions, the use of a dc-link current sensor looks like the best option in order to avoid the offset on it. Nevertheless, a huge disadvantage is observed in this option. Integrated switching power devices (as in the case of this effort) use dc links designed with the objective of minimizing the stray inductances, generally using planar bus bar designs [36]. These kinds of designs preclude the use of current sensor in order to measure dc-link current. Therefore, in this paper, the use of two current sensors was selected.

As a final comment, it is interesting to note the advantage of the first residual ($\mathbf{v}_{\mathrm{HRC}}$) over the second one ($\mathbf{r}_{\mathrm{HRC}}$) with

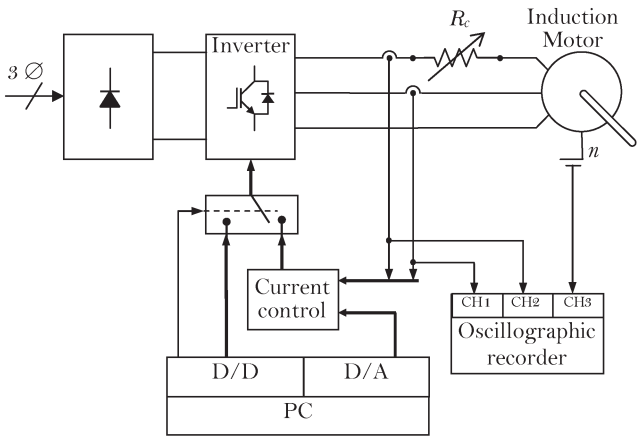

Fig. 9. Experimental setup for validating the proposed HRC method.

respect to offset problems. The first one is not affected by the offset in the voltage sensor, whereas in the second one, the offset in the current sensors must be compensated.

III. Experimental Validation of Proposed Methods

Here, the experimental setup used to validate the methods in Section II is presented together with analytical and experimental results.

A. Experimental Setup

Fig. 9 shows the block diagram of the experimental setup used to validate the proposed diagnosis strategy. The strategy was programmed on a PC, which has a data acquisition card with analog-to-digital and digital-to-analog (D/A) converters and programmable digital inputs/outputs. The switching pattern to the inverter was generated in the PC.

Although the strategy was programmed on a PC, it has a low computational requirement. For this reason, it can be easily implemented in a fixed-point digital signal processor (DSP) of a standard variable speed drive.

The diagnosis strategy was tested in a modified standard 5.5-kW IM, whose rated variables and parameters are provided in Table I. This modified IM was rewinding in order to short-circuit different numbers of turns of the phase a winding. It is well known that the rewinding process increases the inherent asymmetries in the machine, given that it is a handmade process. That is the reason of the important differences between the IM phase resistances.

As it was mentioned in [8], the most common HRC problems occur only in one phase of the incoming circuits of the IM. Therefore, the HRC was emulated with a resistance (R_c) connected in series with IM phase a, as in [8] and [37]. In order to validate the proposed strategy, R_c was set in seven different values during the tests (57.01, 97.21, 218.26, 610.77, 794.71, 976.67, and 1157.6 mΩ). These resistances were measured by an Agilent 34401A digital multimeter with the four-wire resistance measurement method.

Previous values were selected taking the results presented in [8] as a reference, in which the experimental setup has similar characteristics as in this paper. Results about the increment in the contact resistance in a real terminal due to the variation of looseness in the bolt are presented in [8]. The authors consider that selected R_c are reasonable and likely to occur in the real situation, at least in this range of IM power (< 10 kW).

TABLE II
Voltage and Current Sensors Information

Voltage sensor		
Agilent N2772A		
Variable/Parameter	**Value**	**Unit**
Max. primary voltage (V_{pmax})	600	(V)
Accuracy	± 2.5	(%)
Frequency Bandwidth (BW)	20	(MHz)
Current sensors		
HP 1146A		
Primary nominal current rms (I_{pn})	70	(A)
Accuracy	± 4	(%)
Frequency Bandwidth(3dB) (BW)	100	(kHz)

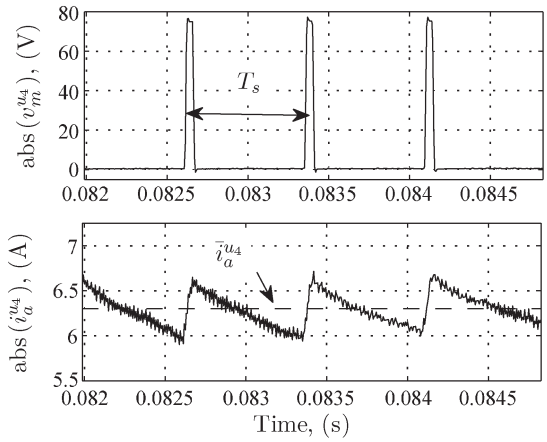

Fig. 10. Time response of v_m and i_a during u_4 injection.

The dc-link negative voltage with respect to the IM neutral point n, i.e., v_m, was logged by an oscillographic recorder (see Fig. 9) with a sampling frequency of 160 kHz and a resolution of 11 bit. In addition, two phase currents were measured and logged with the same instrument. Finally, these signals were analyzed in a PC for obtaining the proposed residuals [see (1) and (3)]. Details about the voltage and current sensors are shown in Table II.

With the experimental setup described above, the results shown in the following section were obtained.

B. Experimental Results

Fig. 10 shows the time response of the absolute value of v_m and i_a when the active state u_4 is injected to the IM, using $R_c = 57.01$ mΩ. In the second figure, the mean value of the current $(\bar{i}_a^{u_4})$ with a maximum current ripple of about 0.6 A is indicated.

Fig. 11 shows the $\mathbf{v}_{\mathrm{HRC}}$ plane where the values of $\mathbf{v}_{\mathrm{HRC}}$ for different R_c are drawn. Some points for R_c were indicated in the figure. As aforementioned in a previous section, HRCs were emulated in phase a. Fig. 11 clearly shows this fact by placing the different points of $\mathbf{v}_{\mathrm{HRC}}$ in a small neighborhood around the axis. Therefore, it is possible to assert that the proposed method is able to identify the faulty phase allowing then rapid troubleshooting.

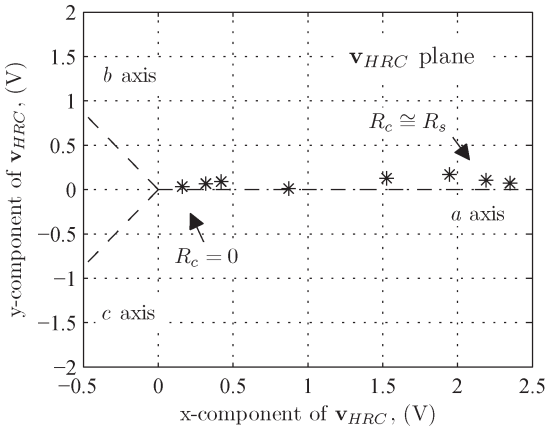

Fig. 11. Variation of $\mathbf{v}_{\mathrm{HRC}}$ with contact resistance in the $\mathbf{v}_{\mathrm{HRC}}$ plane.

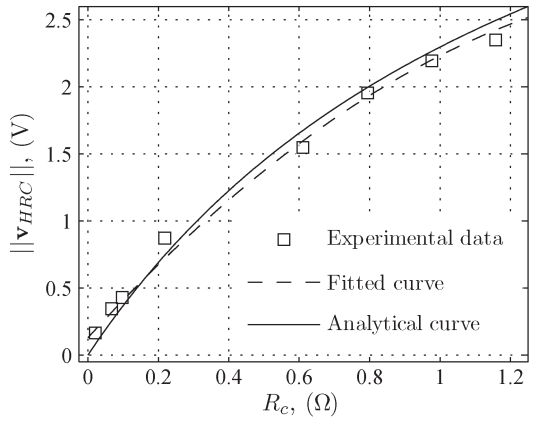

Fig. 12. Euclidean norm of $\mathbf{v}_{\mathrm{HRC}}$ versus contact resistance.

In addition, from Fig. 11, it is possible to note certain inherent asymmetries in the winding phases when $R_c = 0$. Particularly, the IM selected for tests has important inherent asymmetries, as the phase resistances shown in Table I revealed. Despite this fact, results show a very good sensitivity to the variations of R_c, even for its smaller value.

Fig. 12 shows the Euclidean norm of $\mathbf{v}_{\mathrm{HRC}}$ versus R_c. In addition, the fitted curve of the measured data was included and drawn in a dashed line. In order to compare the experimental results with those analytically obtained, a second curve was drawn in the same figure (continuous line). It was calculated considering an HRC in phase a and performing the same methodology used in Section II-C but without considering dead time ($T_d = 0$). Hence, the following values of v_m were used for evaluating (1):

$$\begin{aligned} \bar{v}_m^{u_4} &= V_d D \quad \frac{(2R_s + 2R_c)}{(3R_s + 2R_c)} \\ \bar{v}_m^{u_2} &= V_d D \quad \frac{(2R_s + R_c)}{(3R_s + 2R_c)} \\ \bar{v}_m^{u_6} &= \bar{v}_m^{u_2}. \end{aligned} \tag{13}$$

R_s was set as in Section II-C. Since analytical results were obtained considering symmetric winding resistances, the value of $\|\mathbf{v}_{\mathrm{HRC}}\|$ for $R_c = 0$ is identically zero, whereas experimental results show this asymmetry in the phases.

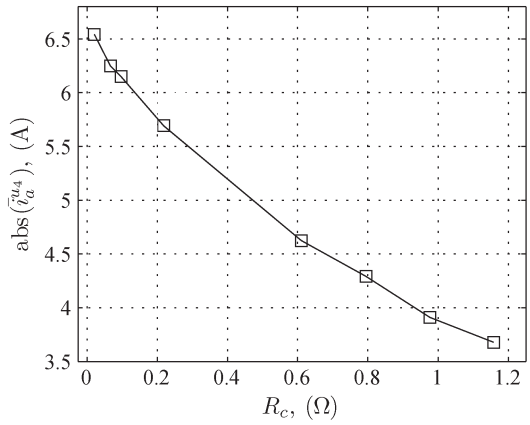

Fig. 13. IM stator current during the inverter u_4 state ($\bar{i}_a^{u_4}$) versus contact resistance.

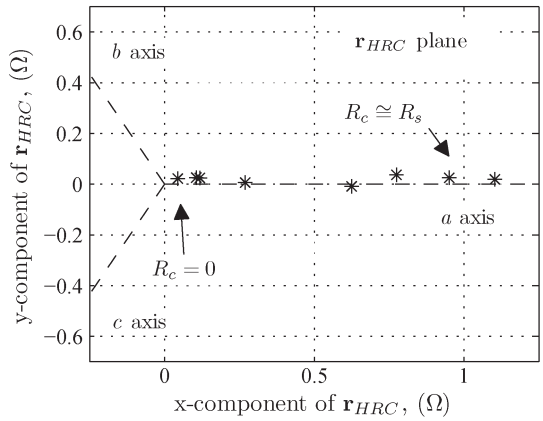

Fig. 14. Variation of $\mathbf{r}_{\mathrm{HRC}}$ with contact resistance in the $\mathbf{r}_{\mathrm{HRC}}$ plane.

Nevertheless, Fig. 12 shows a good correlation between experimental and analytical results as well as the good sensitivity of the proposed method.

The sensitivity of the method depends on the mean value of injected current during the test ($\bar{i}_a^{u_4}$, $\bar{i}_b^{u_6}$, and $\bar{i}_c^{u_2}$). In the present effort, the value of $\bar{i}_x^{u_x}$ was set equal to the RMS value of the stator current of the IM in no-load condition. To do that, the duty cycle was adjusted in $D = 0.1$, whereas the dc-link voltage was $V_d = 100$ V. Fig. 13 shows the absolute values of $\bar{i}_a^{u_4}$ versus the contact resistance. A value equivalent to the no-load stator current is observed for $R_c = 0$.

Although the presented results show the good sensitivity, it could be increased by adjusting the duty cycle of the injected signal in order to equal $\bar{i}_x^{u_x}$ to the rated value of the stator current. Nevertheless, it must be taken into account that this value of current must be injected in a short period of time due to the fact that the IM is at standstill. In this condition, the IM could be seriously damaged due to overheating (if the IM without independent ventilation is considered).

In addition, results for the contact resistance calculated by using a single voltage sensor and phase current information are presented here. Fig. 14 shows the $\mathbf{r}_{\mathrm{HRC}}$ plane in which some points of R_c are indicated. As aforementioned, the proposed method clearly identifies the faulty phase allowing to detect HRC problems.

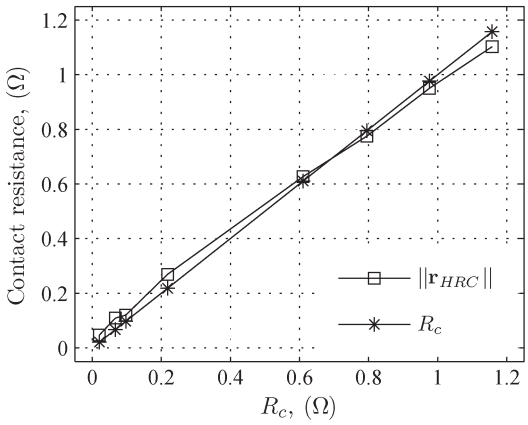

Fig. 15. Contact resistance calculated by the Euclidean norm of $\mathbf{v}_{\mathrm{HRC}}$ and measured with the four-wire method.

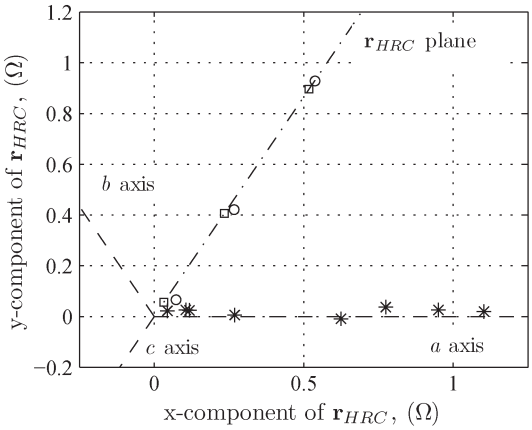

Fig. 16. $\mathbf{r}_{\mathrm{HRC}}$ plane. $(*)$ HRC in phase a. $(\circ)$ $\mathbf{r}_{\mathrm{HRC}}$ with R_{ca} and R_{cb}. $(-\boxdot-)$ $\mathbf{r}_{\mathrm{HRC}}$ calculated with values of R_{ca} and R_{cb} measured with the four-wire method.

Moreover, Fig. 15 compares the Euclidean norm of $\mathbf{r}_{\mathrm{HRC}}$ with R_c, which was measured by the four-wire measurement method. With the proposed method, a good estimation of the contact resistance can be observed. The small differences between the two methods for estimating the contact resistance could be quantified by the percentage relative error calculated as

$$e_r = \left(\frac{R_c - \|\mathbf{r}_{\mathrm{HRC}}\|}{R_c} \right) \times 100\%. \tag{14}$$

The maximum error obtained for the resistance estimation was $e_{\mathrm{r-max}} = 4.9\%$, whereas the average error was $e_{\mathrm{r-avg}} = 2.9\%$. The authors consider that error values are very low for the proposed method, showing its high accuracy in the estimation of HRC problems.

Therefore, it is possible to assert that previous results demonstrate the validity of the proposed method to diagnose problems of HRC.

1) HRC in Two Phases of the IM: As it was mentioned in [8], the most common HRC problems occur in only one phase of the incoming circuits of the IM. Therefore, in previous sections, HRC was emulated with a resistance connected in series with IM phase a, as in [8] and [37].

Despite this fact, here, HRC in two phases of the IM is considered in order to evaluate the validity of the proposed method. In this case, two identical resistances were used and connected to phases a and b. These resistances were identified as R_{ca} and R_{cb}, and their values were set as $R_{ca} = R_{cb} = (57.01, 441.0, 1009.0)$ mΩ.

Fig. 16 shows the $\mathbf{r}_{\mathrm{HRC}}$ plane in which the results obtained with the proposed method for HRC in two phases are indicated with $(\circ)$. In addition, the residual was also calculated with the values of resistances measured with the four-wire method. These results are indicated in the figure with squares and connected by a dash-dotted line $(-\boxdot-)$ $\mathbf{r}_{\mathrm{HRC}}$. In order to compare these results with those previously obtained for HRC in one phase, they were also incorporated in this figure, indicated by $(*)$.

By analyzing Fig. 16, it is noticed that experimental results, which are obtained with HRC in two phases, are placed in a small neighborhood around the bisector line between axes a and b (exactly $2\pi/6$ rad). It can be easily explained by taking into account that the geometrical composition of two vectors with the same Euclidean norm is always on the bisector line.

Based on these results, it is possible to assert that, in a general case, in which $R_{ca} \neq R_{cb}$, the proposed method will place points in a sector of the $\mathbf{r}_{\mathrm{HRC}}$ plane limited by axes a and b. The exact point will be given by the Euclidean norm and the angle of $\mathbf{r}_{\mathrm{HRC}}$, which can be calculated as

$$\zeta_{\mathbf{r}_{\mathrm{HRC}}} = \mathrm{atan2}\left(\mathbf{r}_{\mathrm{HRC}}(\text{x-comp}), \mathbf{r}_{\mathrm{HRC}}(\text{y-comp})\right). \tag{15}$$

The angle ζ allows identifying the faulty phases as well as rapid and precise troubleshooting for HRC in two phases.

Finally, it is important to point out the good correlation between experimental and analytical results, as in the case of HRC in one phase, validating in this way the proposed method for the case of HRC in two phases.

IV. Proposed FDI Algorithm

Here, an FDI algorithm for the diagnosis of HRC is proposed.

Fig. 17(a) shows the block diagram schematizing the proposed FDI algorithm. The first step for the detection of HRC consists in the measurement of voltage or voltage and currents, as well as in the preprocessing of that signals in order to avoid offset. A second step involves the computation of proposed residuals, i.e., (1) or (3), depending on measured signals.

Once the residuals are calculated, the Euclidean norm $(\| \bullet \|)$ is taken and compared with limits ($\boldsymbol{\lambda}_{\|\mathbf{v}_{\mathrm{HRC}}\|}$ or $\boldsymbol{\lambda}_{\|\mathbf{r}_{\mathrm{HRC}}\|}$) for detecting and quantifying the HRC. If $\| \bullet \| > \boldsymbol{\lambda}$, the algorithm will return the faulty condition as the healthy one.

In addition, after the faulty condition is returned, the angle ζ is enabled to be computed by using (15). Based on this information, it is possible to determine the faulty phases in which HRC appears.

The following sections show how to determine the limits $\boldsymbol{\lambda}$ and the phases affected by the HRC.

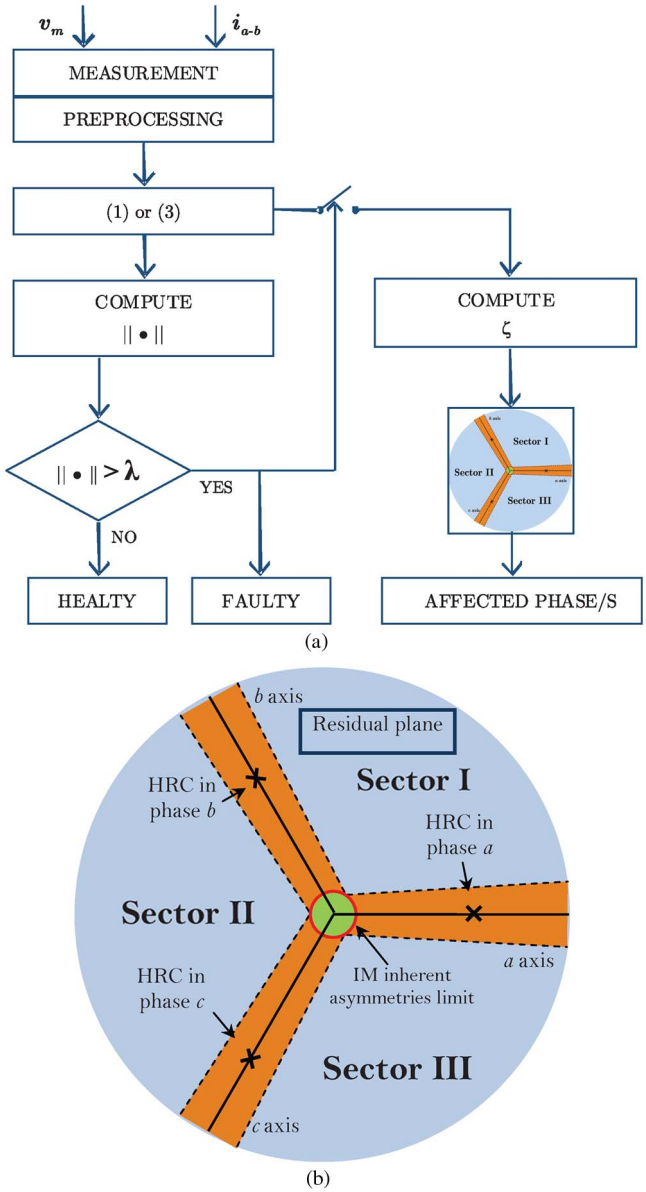

Fig. 17. FDI algorithm. (a) Block diagram and (b) limits for the HRC alarms.

A. Determination of Limits for the HRC Alarms ($\boldsymbol{\lambda}$)

This section presents a brief description of how to determine the limits for the HRC alarms, i.e., $\boldsymbol{\lambda}$.

By measuring the stator resistances of 15 new IMs, the authors could determine a maximum inherent asymmetry of 1.5% of the mean value between R_{sa}, R_{sb}, and R_{sc}. These values can be taken as a reference for low-power machines (all tested IMs belong to this range of power, i.e., < 10 kW).

This way, the following limit for $\|\mathbf{r}_{\mathrm{HRC}}\|$ is proposed:

$$\boldsymbol{\lambda}_{\|\mathbf{r}_{\mathrm{HRC}}\|} = 1.5 \times \mathrm{mean}\left([R_{sa}, R_{sb}, R_{sc}]\right)/100. \tag{16}$$

For determining $\boldsymbol{\lambda}_{\|\mathbf{v}_{\mathrm{HRC}}\|}$, the use of (16) is proposed, yielding

$$\boldsymbol{\lambda}_{\|\mathbf{v}_{\mathrm{HRC}}\|} = \boldsymbol{\lambda}_{\|\mathbf{r}_{\mathrm{HRC}}\|} * \bar{i}_x^{u_x} \tag{17}$$

TABLE III
AFFECTED PHASES DEPENDING ON ANGLE ζ

Angle limits	Sector	Affected phase/s
$0 < \zeta < 2\pi/3$	I	a and b
$2\pi/3 < \zeta < 4\pi/3$	II	b and c
$4\pi/3 < \zeta < 2\pi$	III	c and a
$\zeta = 0$	-	a
$\zeta = 2\pi/3$	-	b
$\zeta = 4\pi/3$	-	c

where $\bar{i}_x^{u_x}$ is the mean value of injected current during the test. This reference current is selected in order to obtain the highest sensitivity in the method, as it was pointed out in Section III-B.

These limits set the radius of the red circumference indicated as "*IM inherent asymmetries limit*" in Fig. 17.

B. Determination of Phases in Which HRC Occurs

In order to identify the phases in which HRC occurs, the angle ζ must be computed. This value will be allocated in one of the three sectors in which the residual plane was divided (see Fig. 17).

Once the sector is identified, it is possible to determine the faulted phases. Table III shows the angle limits of the sectors as well as the phases, which are affected by HRC in each sectors.

In addition, bands along the phase axes are taken into account in order to avoid false identification as a product of inherent asymmetries of the IM (see Fig. 17). These inherent asymmetries can cause ζ to deviate from 0 for an HRC in phase a, $2\pi/3$ for phase b, or $4\pi/3$ for phase c.

These limits are set in the value selected for λ with a small slop, in order to take into account the dispersion produced when the phase current decreases as a product of an increment in the HRC.

V. Conclusion and Final Remarks

Two new automatic HRC diagnosis methods based on signal injection have been proposed in this effort. The theoretical underpinning of these two offline diagnosis methods was presented, showing a detailed description of the predefined injected signal as well as two HRC residuals. Both residuals need the information of the voltage in the neutral point of the machine. One of them ($\mathbf{v}_{\mathrm{HRC}}$) is calculated by using a single voltage sensor, being immune to offset problems in the sensor. The other residual ($\mathbf{r}_{\mathrm{HRC}}$) uses the voltage provided by this sensor plus the stator current information.

Both methods were experimentally validated using a laboratory prototype. The possibility of detecting HRCs while determining their severity was demonstrated. In addition, the physical location of the HRC in the incoming circuit of the IM with both indicators was demonstrated even for HRC in two phases. All this information was obtained with a very low estimation error and a high immunity to symmetric variations in the IM stator resistance and those associated to the inverter.

Finally, an FDI algorithm to implement the proposed HRC diagnosis method has been put forward. Details about the selection of the limits for HRC alarms were presented.

These simple methods can be programmed in the DSP of the standard drive since they do not need large computational requirements nor database information of the IM. These two low-cost automatic HRC diagnosis methods only need an additional single voltage sensor since the current information is usually available in a standard IM drive.

In addition, it can be noted that the proposed HRC diagnosis methods use the same experimental arrangement previously presented in literature for diagnosing stator winding turn faults. Therefore, these faults could be also detected and isolated in order to obtain a more accurate diagnosis.

ACKNOWLEDGMENT

The authors would like to thank M. Otero for his assistance during the experimental tests.

REFERENCES

[1] S. Grubic, J. M. Aller, B. Lu, and T. G. Habetler, "A survey on testing and monitoring methods for stator insulation systems of low-voltage induction machines focusing on turn insulation problems," *IEEE Trans. Ind. Electron.*, vol. 55, no. 12, pp. 4127–4136, Dec. 2008.

[2] A. Bellini, F. Filippetti, C. Tassoni, and G.-A. Capolino, "Advances in diagnostic techniques for induction machines," *IEEE Trans. Ind. Electron.*, vol. 55, no. 12, pp. 4109–4126, 2008.

[3] M. Ben Khader Bouzid and G. Champenois, "New expressions of symmetrical components of the induction motor under stator faults," *IEEE Trans. Ind. Electron.*, vol. 60, no. 9, pp. 4093–4102, Sep. 2013.

[4] M. Prieto, G. Cirrincione, A. Espinosa, J. Ortega, and H. Henao, "Bearing fault detection by a novel condition-monitoring scheme based on statistical-time features and neural networks," *IEEE Trans. Ind. Electron.*, vol. 60, no. 8, pp. 3398–3407, Aug. 2013.

[5] H. Henao, C. Demian, and G.-A. Capolino, "A frequency-domain detection of stator winding faults in induction machines using an external flux sensor," *IEEE Trans. Ind. Appl.*, vol. 39, no. 5, pp. 1272–1279, Sep./Oct. 2003.

[6] K. Lee, J. Hong, K. Lee, S.-B. Lee, and E. Wiedenbrug, "A stator core quality assessment technique for inverter-fed induction machines," *IEEE Trans. Ind. Appl.*, vol. 46, no. 1, pp. 213–221, Jan./Feb. 2010.

[7] I. Georgakopoulos, E. Mitronikas, and A. Safacas, "Detection of induction motor faults in inverter drives using inverter input current analysis," *IEEE Trans. Ind. Electron.*, vol. 58, no. 9, pp. 4365–4373, Sep. 2011.

[8] J. Yun, J. Cho, S. B. Lee, and J.-Y. Yoo, "Online detection of high-resistance connections in the incoming electrical circuit for induction motors," *IEEE Trans. Ind. Appl.*, vol. 45, no. 2, pp. 694–702, Mar./Apr. 2009.

[9] M. Braunovic, N. Myshkin, and V. Konchits, *Electrical Contacts: Fundamentals, Applications and Technology*. New York, NY, USA: Taylor & Francis, 2006.

[10] V. Babrauskas, "How do electrical wiring faults lead to structure ignitions?" in *Proc. Fire Mater. Conf.*, London, U.K., 2001, pp. 39–51.

[11] R. Tallam, T. Habetler, and R. Harley, "Stator winding turn-fault detection for closed-loop induction motor drives," *IEEE Trans. Ind. Appl.*, vol. 39, no. 3, pp. 720–724, May/Jun. 2003.

[12] F. Briz, M. Degner, J. Guerrero, and P. Garcia, "Stator windings fault diagnostics of induction machines operated from inverters and soft-starters using high-frequency negative-sequence currents," *IEEE Trans. Ind. Appl.*, vol. 45, no. 5, pp. 1637–1646, Sep./Oct. 2009.

[13] S. Cheng, P. Zhang, and T. Habetler, "An impedance identification approach to sensitive detection and location of stator turn-to-turn faults in a closed-loop multiple-motor drive," *IEEE Trans. Ind. Electron.*, vol. 58, no. 5, pp. 1545–1554, May 2011.

[14] V. Leši, M. Vašak, M. Gulin, N. Peri, G. Joksimovi, and T. M. Wolbank, "Field-oriented control of an induction machine with winding asymmetries," in *Proc. 15th Int. EPE-PEMC Conf./ECCE*, Novi Sad, Serbia, 2012, pp. LS7b-1.2-1–LS7b-1.2-7.

[15] S. B. Lee, J. Yang, J. Hong, J.-Y. Yoo, B. Kim, K. Lee, J. Yun, M. Kim, K.-W. Lee, E. Wiedenbrug, and S. Nandi, "A new strategy for condition monitoring of adjustable speed induction machine drive systems," *IEEE Trans. Power Electron.*, vol. 26, no. 2, pp. 389–398, Feb. 2011.

[16] A. Soualhi, G. Clerc, and H. Razik, "Detection and diagnosis of faults in induction motor using an improved ant clustering technique," *IEEE Trans. Ind. Electron.*, vol. 60, no. 9, pp. 4053–4062, Sep. 2013.

[17] Z. Zhu and L. Gong, "Investigation of effectiveness of sensorless operation in carrier-signal-injection-based sensorless-control methods," *IEEE Trans. Ind. Electron.*, vol. 58, no. 8, pp. 3431–3439, Aug. 2011.

[18] R. Leidhold, "Position sensorless control of PM synchronous motors based on zero-sequence carrier injection," *IEEE Trans. Ind. Electron.*, vol. 58, no. 12, pp. 5371–5379, Dec. 2011.

[19] E. Al-nabi, B. Wu, N. R. Zargari, and V. Sood, "Sensorless control of CSC-fed IPM machine for zero- and low-speed operations using pulsating HFI method," *IEEE Trans. Ind. Electron.*, vol. 60, no. 5, pp. 1711–1723, May 2013.

[20] G. Wang, R. Yang, and D. Xu, "DSP-based control of sensorless IPMSM drives for wide-speed-range operation," *IEEE Trans. Ind. Electron.*, vol. 60, no. 2, pp. 720–727, Feb. 2013.

[21] F. Briz and M. Degner, "Rotor position estimation," *IEEE Ind. Electron. Mag.*, vol. 5, no. 2, pp. 24–36, Jun. 2011.

[22] R. Morales-Caporal and M. Pacas, "Suppression of saturation effects in a sensorless predictive controlled synchronous reluctance machine based on voltage space phasor injections," *IEEE Trans. Ind. Electron.*, vol. 58, no. 7, pp. 2809–2817, Jul. 2011.

[23] G. R. Bossio, C. H. De Angelo, J. A. Solsona, G. O. Garcia, and M. I. Valla, "Application of an additional excitation in inverter-fed induction motors for air-gap eccentricity diagnosis," *IEEE Trans. Energy Convers.*, vol. 21, no. 4, pp. 839–847, Dec. 2006.

[24] G. R. Bossio, C. H. De Angelo, G. O. Garcia, J. A. Solsona, and M. I. Valla, "Effects of rotor bar and end-ring faults over the signals of a position estimation strategy for induction motors," *IEEE Trans. Ind. Appl.*, vol. 41, no. 4, pp. 1005–1012, Jul./Aug. 2005.

[25] F. Briz, M. Degner, P. Garcia, and A. Diez, "High-frequency carrier-signal voltage selection for stator winding fault diagnosis in inverter-fed ac machines," *IEEE Trans. Ind. Electron.*, vol. 55, no. 12, pp. 4181–4190, Dec. 2008.

[26] G. Bossio, C. De Angelo, P. de la Barrera, J. Solsona, G. Garcia, and M. Valla, "Stator winding fault detection in induction motor drives using signal injection," in *Proc. IEEE Int. SDEMPED*, Sep. 2011, pp. 92–97.

[27] P. de la Barrera and G. Bossio, "Stator core faults detection on induction motor drives using signal injection," in *Proc. IEEE Int. SDEMPED*, Sep. 2011, pp. 98–104.

[28] M. Baranski and A. Polak, "Thermal diagnostic in electrical machines," *PRZEGLAD ELEKTROTECHNICZNY (Elect. Rev.)*, vol. 10, pp. 305–308, Oct. 2011.

[29] R. Colby, "Detection of high-resistance motor connections using symmetrical component analysis and neural network models," in *Proc. 4th IEEE Int. SDEMPED*, Aug. 2003, pp. 2–6.

[30] J. Bockstette, E. Stolz, and E. Wiedenbrug, "Upstream impedance diagnostic for three-phase induction motors," in *Proc. IEEE Int. SDEMPED*, Sep. 2007, pp. 411–414.

[31] J. Yun, K. Lee, K.-W. Lee, S. B. Lee, and J.-Y. Yoo, "Detection and classification of stator turn faults and high-resistance electrical connections for induction machines," *IEEE Trans. Ind. Appl.*, vol. 45, no. 2, pp. 666–675, Mar./Apr. 2009.

[32] L. Zarri, M. Mengoni, Y. Gritli, A. Tani, F. Filippetti, G. Serra, and D. Casadei, "Detection and localization of stator resistance dissymmetry based on multiple reference frame controllers in multiphase induction motor drives," *IEEE Trans. Ind. Electron.*, vol. 60, no. 8, pp. 3506–3518, Aug. 2013.

[33] Y. Gritli, L. Zarri, C. Rossi, F. Filippetti, G. Capolino, and D. Casadei, "Advanced diagnosis of electrical faults in wound-rotor induction machines," *IEEE Trans. Ind. Electron.*, vol. 60, no. 9, pp. 4012–4024, Sep. 2013.

[34] N. Urasaki, T. Senjyu, K. Uezato, and T. Funabashi, "Adaptive dead-time compensation strategy for permanent magnet synchronous motor drive," *IEEE Trans. Energy Convers.*, vol. 22, no. 2, pp. 271–280, Jun. 2007.

[35] A. Somani, R. Gupta, K. Mohapatra, and N. Mohan, "On the causes of circulating currents in PWM drives with open-end winding ac machines," *IEEE Trans. Ind. Electron.*, vol. 60, no. 9, pp. 3670–3678, Sep. 2013.

[36] M. Caponet, F. Profumo, R. De Doncker, and A. Tenconi, "Low stray inductance bus bar design and construction for good EMC performance in power electronic circuits," *IEEE Trans. Power Electron.*, vol. 17, no. 2, pp. 225–231, Mar. 2002.

[37] D. Patel and M. Chandorkar, "On-line load test for induction machine stator inter-turn fault detection under stator electrical asymmetries," in *Proc. 36th Annu. Conf. IEEE IECON*, Nov. 2010, pp. 933–938.

Pablo M. de la Barrera (S'99–GS'08–M'09) was born in Rio Cuarto, Argentina, in 1978. He received the B.Sc. and M.Sc. degrees in electrical engineering from the Universidad Nacional de Rio Cuarto, Rio Cuarto, in 2003 and 2006, respectively, and the Ph.D. degree in control systems from the Universidad Nacional del Sur, Bahía Blanca, Argentina, in 2009.

Since 1998, he has been with the Grupo de Electrónica Aplicada, Universidad Nacional de Río Cuarto. He is also currently with the Consejo Nacional de Investigaciones Científicas y Técnicas (CONICET), Buenos Aires, Argentina.

Dr. de la Barrera is currently the Secretary of the Argentina Section Joint Chapter within the IEEE (IE13/CS23/RA24/IA34/PEL35/VT06).

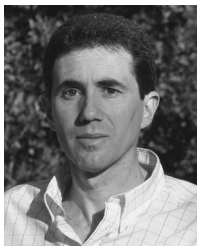

Guillermo R. Bossio (S'03–M'07) received the B.Sc. degree in electrical engineering from the Universidad Nacional de Río Cuarto, Rio Cuarto, Argentina, in 1999, and the Ph.D. degree in engineering from the Universidad Nacional de La Plata, La Plata, Argentina, in 2004.

Since 1994, he has been with the Grupo de Electronica Aplicada, Facultad de Ingeniera, Universidad Nacional de Rio Cuarto. He is also currently with the Consejo Nacional de Investigaciones Cientificas y Tecnicas, Buenos Aires, Argentina. His research interests include fault diagnosis on electric machines, ac motor drives, electric vehicles, and renewable energy generation.

Jorge A. Solsona (SM'04) received the B.Sc. degree in electronic engineering and the Dr. Eng. degree from the Universidad Nacional de La Plata, La Plata, Argentina, in 1986 and 1995, respectively.

He is currently a Professor with the Departamento de Ingeniera Electrica y de Computadoras, Instituto de Investigaciones en Ingeniera Electrica "Alfredo C. Desages," Universidad Nacional del Sur, Bahia Blanca, Argentina. He is also currently with the Consejo Nacional de Investigaciones Cientificas y Tecnicas, Buenos Aires, Argentina. He is involved in teaching and research on control theory and its applications to electromechanical systems.